Chapter 3

Spontaneous exchange bias and large dielectric constant in $Bi_{0.8}Tb_{0.2}Fe_{0.8}Mn_{0.2}O_3$ multiferroic

3.1 INTRODUCTION

The spontaneous exchange bias or zero field-cooled exchange bias (ZEB) has drawn a lot of consideration since the unidirectional anisotropy (UA) creates all alone, even though the material is not cooled in a field through Neel temperature (T_N)[66,67]. It is important to mention that the zero-field cooled (ZFC) isothermal magnetization (M-H) loop displays a major change across the magnetic field axis that has not been yet seen in any conventional exchange bias (CEB; H_{CEB}) of bulk BFO system at room temperature (RT). Former investigations have revealed exceptional spontaneous exchange bias in many systems including $BiFeO_3$-$CoFe_2O_4$ nanocomposites[68], $Pr_2CoMn_{0.5}Fe_{0.5}O_6$[69], $La_{1.5}Sr_{0.5}Co_{1-x}Fe_xMnO_6$[55], $LaFeO_3$ nanoparticles[70], and Mn_2PtGa[71]. From both theoretical and technological perspectives, the occurrence of exchange bias (EB) has received a lot of attention. The EB effect is associated with an exchange anisotropy in a variety of geometries, which would include core-shell nanostructures, granular composites, bilayers, and superlattices, involving ferromagnetic (FM) / antiferromagnetic (AFM) interfaces, FM / ferrimagnets (FiM), FM/spin glass (SG), and hard/soft FM systems in a variety of geometries[72]. According to several studies, dilution of the AFM portion due to nonmagnetic substitution (e.g., $Co_{1-x}Mg_xO$) or defects (e.g., $Co_{1-y}O$) have a significant impact on the exchange bias characteristics of an FM-AFM system[73]. There are few studies of EB in AFM- two-dimensional diluted antiferromagnet shell (2D DAFF) systems in the literature [74]. In Co_3O_4, CoO, and Cr_2O_3 nanostructures with an AFM core–2D DAFF shell configuration, Benitez et al. has recently observed a shifted field-cooled (FC) hysteresis loop[75]. The main objectives for researchers are to make the most elevated use of the EB from an application point of view[76]. Investigations of spontaneous loop change in nanoparticles and layer structures below the blocking temperature without the use of an

external magnetic field have recently emerged [77]. The spontaneous exchange bias phenomenon is the result of an unforeseen zero-field cooled M–H loop shift without pre-biasing[78]. A minor exchange bias loop shifting upon ZFC was previously thought to be an artifact; however, Saha et al. have developed a model for a modest but inherent phenomenon in the $Ni_{80}Fe_{20}/Ni_{50}Mn_{50}$ system[79]. Since the spontaneous exchange bias effect eliminates the need for an external magnetic field to achieve unidirectional anisotropy, it will be of enormous importance in the electric field control of exchange bias-based devices and much other application purposes[80].

Out of the identified multiferroic (MF) materials, only $BiFeO_3$ (BFO) possesses both G-type canted antiferromagnetism (Neel temperature T_N = 643 K) and ferroelectricity (Curie temperature T_C = 1103 K) consequently above ambient temperature[81,82]. $BiFeO_3$ is one of the most explored MF materials, some experimental and first-principle calculations suggested that $BiFeO_3$ MF properties would be promising for huge applications in magnetoelectric devices with electrically controlled magnetism. High leakage current density, high dielectric loss, secondary phase impurities, chemical fluctuations, poor ME coupling, and inhomogeneous magnetic spin structure are all obstacles that must be overcome before BFO-based devices can be created commercially viable.[83] Although $BiFeO_3$ is a well-studied system in the literature with different doping, however, room temperature ferromagnetism is still less explored in this system.

In this article, we choose Terbium (Tb) as a dopant at the A-site due to its high magnetic moment (9.72 μB/mol)[84], which might also strengthen magnetic order as previously observed in $TbFeO_3$[85]. Furthermore, Tb doping can also strengthen magnetoelectric (ME) coupling which is a limitation of type- I (BFO) multiferroic materials. Terbium ions (Tb^{3+}) are the most appropriate dopant at the A site due to their large atomic weight, smaller size

than Bi ions (Bi^{3+}), and similar electro-negativity to Bi^{3+}. Tb ionic radius is smaller than the Bi ion which will create internal lattice pressure inside the material and as a result, significant structural distortions are expected[84,86]. The ionic radii of component elements must match properly for a perovskite structure (ABO_3) to be stable. The tolerance factor is predicted to be reduced when tiny Tb^{3+} ions are introduced into BFO perovskite because the average A-site ionic radius is reduced. Since certain ions have a smaller ionic radius, the Fe–O–Fe bond angle bends more, resulting in a decreased tolerance factor and a more insulated character. As a result, the Fe^{3+}–O^{2+}–Fe^{3+} bond angle changes from 180 degrees. For high spin eight-fold coordination, the ionic radii of Bi^{3+} and Tb^{3+} are 1.17Å and 1.06 Å, respectively, whereas the ionic radii of $Fe^{3+}$and Mn^{3+} are similar (0.785 Å) for high spin six-fold coordination[87,88]. Any sort of magnetoelectric (ME) coupling would thus be increased at a transition temperature, and reducing either T_N or T_C to around room temperature is one method for obtaining a material with a strong magnetoelectric effect at room temperature. Wang et al. have investigated Mn-doped BFO to establish a mixed Fe valence (i.e. Fe^{3+} and Fe^{2+}) due to the substitution of Mn. With increasing doping, the T_N is shifted towards lower temperatures, and the magnetic intensities increase almost linearly with decreasing temperature[89].

3.2 EXPERIMENTAL DETAILS

The chemical compositions of sample $Bi_{0.8}Tb_{0.2}Fe_{0.8}Mn_{0.2}O_3$ (BTFMO82) were synthesized by the conventional solid-state reaction method. High purity oxides viz. Bi_2O_3, Fe_2O_3, Tb_4O_7, and Mn_2O_3 were grounded in the stoichiometric ratio[90]. Structural analysis of the sample was carried out with the help of an X-ray diffractometer (XRD), measured using Rigaku miniflex – II Cu K_α radiation (λ=1.5406 Å) with a step size of 0.02 and a scan rate of 2^o per minute, in the range of Bragg angles 2θ ($20 \leq 2\theta \leq 80$) at RT. Label and Rietveld refinement of X-ray powder diffraction data was done with FULLPROF suite

software. In the temperature range of 5-300 K, the magnetic measurement was performed with a Quantum Design MPMS-3 magnetometer. The magnetic measurement of the sample at a high temperature (300- 650 K) was performed with the help of a vibrating magnetometer (VSM). An Omicron multi-probe surface science system was used for the XPS experiment, which used a monochromatic X-ray source Al-K_α line with a photon energy of 1486.7 eV. A hemispheric electron energy analyzer is included in the system (EA 125). $5.6x10^{-10}$ torr was the average base pressure for the experiment. The neutron diffraction measurements were performed using a PD2 neutron powder diffractometer (λ = 1.2443 Å) at the Dhruva reactor of the Atomic Research Centre in Mumbai, India. Raman spectra have been captured at room temperature (Model: LabRAM HR Evolution, Horiba Ltd, Japan) using a 633 nm laser excitation.

3.3 RESULTS AND DISCUSSION

3.3.1 X-RAY DIFFRACTION STUDY:

Figure 3.1 shows the room temperature X-ray diffraction (XRD) patterns of the polycrystalline BTFMO82. To investigate the impact of Tb and Mn substitution in BFO, a careful examination of XRD patterns was carried out. The crystallographic studies of the XRD data were carried out using the FULLPROF program and the Rietveld refinement technique. A pseudo-Voigt function was used to improve the peak forms, and a six-coefficient polynomial function was used to simulate the background. The orthorhombic Pnma structure is known in the parent compound $TbMnO_3$. Whereas, our system has a diffraction profile that was found to be very similar to orthorhombic TbFeO3.[85] The structure of $Pn2_1a$+Pnma (orthorhombic) space groups is being used to refine the XRD pattern of prepared materials.

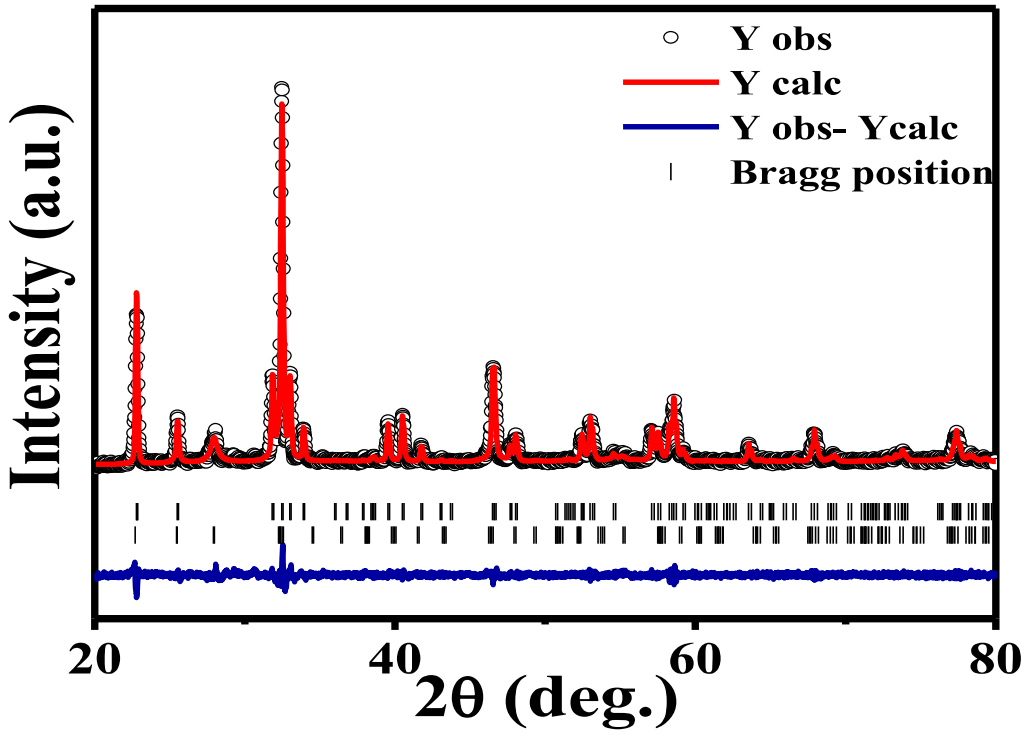

Figure 3.1: *Rietveld refinement of the X-ray diffraction data of* $Bi_{0.8}Tb_{0.2}Fe_{0.8}Mn_{0.2}O_3$ *system.*

The sample has been completely fitted by the above space groups confirming the absence of any impurity peak. The XRD data show that BTFMO82 develops into the orthorhombic ($Pn2_1a$+Pnma) phase through an intermediate two-phase state that occurs across a large concentration range of $0.10 \leq x \leq 0.20$. Considering that the polar R3c phase is primarily responsible for ferroelectricity and the non-polar Pnma phase is only responsible for increasing magnetization.[91]

3.3.2 NEUTRON DIFFRACTION STUDY:

Neutron powder diffraction (NPD) experiments were carried out at different temperatures ranging from 6 K to 300 K to validate the magnetic transition temperature and the magnetic structure of BTFMO82. The refined structural parameters obtained from the NPD have

summarized in Table 1. Figure 3.2(a) shows the Rietveld refined NPD patterns in the (6 K – 300 K) temperature range. No satellite peak is observed at all temperature ranges (6 K-300 K). From the NPD data study, we found that crystal structure does not change in the temperature range of 6 K–300 K.

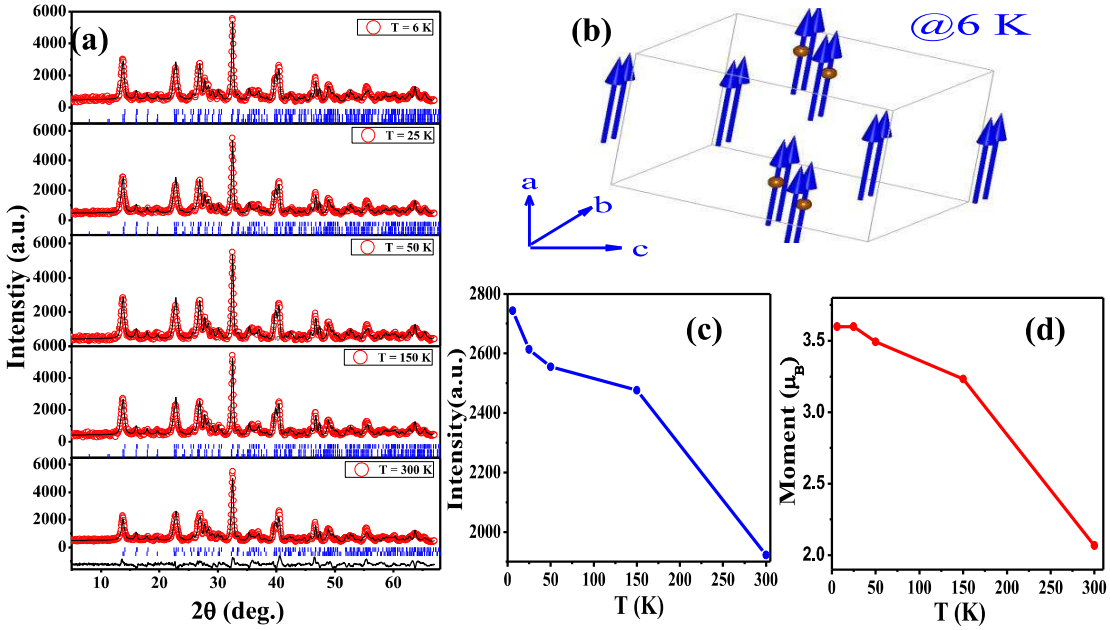

Figure 3.2: *(a)The Rietveld refined neutron powder diffraction pattern of $Bi_{0.8}Tb_{0.2}Fe_{0.8}Mn_{0.2}O_3$ at 300 K,150 K, 50 K, 25 K, and 6 K. (b) Ferromagnetic type structure generated from Rietveld refinement of neutron powder diffraction at 6 K. (c) Variation of peak intensity with the temperature at 2Θ = 13.74 deg. (d) Variation of magnetic moment (μ_B) with temperature.*

Table 1: *Structural parameters and crystallographic sites determined from Rietveld profile refinement of the NPD for BTFMO82 at 6 K and 300 K. Space group: Pnma and Pn21a.*

All the obtained NPD data are properly refined by the orthorhombic phase with space group Pnma and $Pn2_1a$ which supports XRD data. Moreover, the NPD data were also refined successfully with both nuclear (Pnma and $Pn2_1a$) and magnetic (P-1) phases present at all temperatures. At 6 K magnetic moment is 3.6 μ_B and the magnetic structure at this temperature is ferromagnetic as shown in figure 3.2(b). Around angle 2Θ (deg) = 13.74,

peak intensity increases as temperature decreases as shown in figure 3.2(c). Figure 3.2(d) illustrates the pictorial representation of temperature vs magnetic moment; magnetic moment decreases as temperature increases. Thus, both the crystal structure and the magnetic ordering of BFO are significantly altered by co-doping. From this study, we found that there is more bulking in bond angle and non-zero moment observed at room temperature.

	6 K		300 K	
NPD data recorded at	Pnma	$Pn2_1a$	Pnma	$Pn2_1a$
a (Å)	5.607 794	5.502 486	5.615 746	5.529 272
b (Å)	7.795 310	7.866 019	7.793 525	7.879 040
c (Å)	5.439 799	5.598 945	5.436 998	5.609 311
Bi/Tb				
X	0.008 60	0.419 07	0.006 04	0.419 07
Y	0.781 51	0.037 21	0.784 23	0.037 21
Z	1.033 04	−0.194 45	1.035 20	−0.194 45
Fe/Mn				
X	0.193 53	−0.032 42	0.192 20	−0.032 42
Y	0.082 22	0.371 67	0.078 96	0.371 67
Z	1.268 78	−0.300 86	1.273 11	−0.300 86
O(1)				
X	0.458 80	−0.270 98	0.457 13	−0.270 98
Y	0.217 39	0.155 56	0.214 18	0.155 56
Z	0.018 79	−0.015 02	0.019 34	−0.015 02
O(2)				
X	0.456 55	−0.274 53	0.454 73	−0.274 53
Y	0.002 60	−0.209 36	0.000 66	−0.209 36
Z	0.002 34	0.389 91	0.002 63	0.389 91
O(3)				
X	0.305 69		0.312 30	
Y	0.058 81		0.054 34	
Z	0.320 15		0.324 65	
Bond length				
Bi/Tb–O1	2.636 2	2.818 6	2.626 8	2.825 3
Bi/Tb–O2	2.695 4	2.832 3	2.695 0	2.839 7
Bi/Tb–O3	2.332 3		2.333 3	
Fe/Mn–O1	2.044 1	2.162 8	2.046 3	2.169 4
Fe/Mn–O2	1.923 9	2.371 3	1.926 3	2.377 9
Fe/Mn–O3	2.235 5		2.241 4	
Bond angle				
Mn/Fe–O_1–Fe/Mn (deg)	149.619	150.22	149.95	150.65
Mn/Fe–O_2–Fe/Mn (deg)	148.17	150.20	148.82	150.21
Mn/Fe–O_3–Fe/Mn (deg)	150.57		150.30	

3.3.3 RAMAN SPECTROSCOPY STUDY:

Raman spectroscopy can be used to analyze the detailed information about the local lattice dynamics/disorder of the systems micro and macrophases[92,93]. The Raman spectra of the BTFMO82 system-was obtained at room temperature as shown in figure 3. According to the theoretical study, pure $BiFeO_3$ shows eighteen (18) optical phonon modes(Γ_{opt}) as Γ_{opt}= $4A_1 + 5A_2 + 9E$, where A_1 (4) and E(9) modes (13) are both Raman active and A_2 (5) modes are infrared active-for rhombohedral distorted R3c BFO.[94,95] Lattice deformation and local strain fields produced by partial substitution may cause shifting in some of the modes.[96]

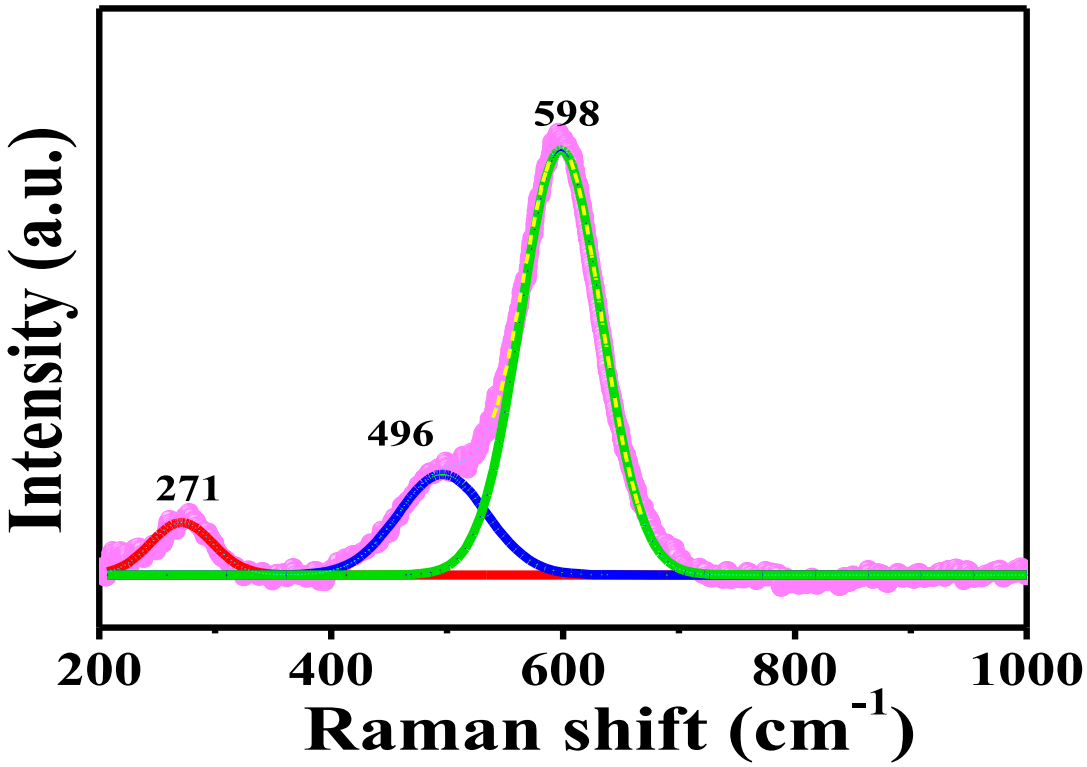

Figure 3.3: *Room-temperature micro-Raman spectra of $Bi_{0.8}Tb_{0.2}Fe_{0.8}Mn_{0.2}O_3$ system.*

In the range of 10 cm^{-1} to 1000 cm^{-1}, we have recorded precisely four prominent Raman broad peaks at~ 271, 496, and 598 cm^{-1} for $Bi_{0.8}Tb_{0.2}Fe_{0.8}Mn_{0.2}O_3$ as shown in Fig. 3.3. The A_1 modes and low-frequency E modes below 400 cm^{-1} for $BiFeO_3$ are related to Bi-O bonds that are responsible for the ferroelectric activity, whereas higher frequency E modes are associated with Fe-O bonds. The weak band at 496 cm^{-1} originated might be-due to the

bending vibration of the Fe/MnO_6 octahedron, which has been described in perovskites. The Raman active modes at 271 cm^{-1} and 598 cm^{-1} are generated by anti-stretching and stretching vibrations, respectively.[97,98] Xie Y. et al. showed the Raman spectra of BFO and $Bi_{0.9}Gd_{0.1}Fe_{1-x}Cr_xO_3$ (x = 0, 0.025, 0.05, 0.075, 0.10) thin films at room temperature, explaining that with an increase in doping concentration, some active modes disappeared and some active mode got shifted toward higher frequency compared to BFO.[99] T. Wang et al. did comparative studies of pure BFO and Co-doped samples and found the difference in Raman data, which is the indication of structural change and more distortion in BFO lattice, which is also true for our BTFMO82 system and it supports the XRD and neutron data described earlier.[100]

3.3.4 DIELECTRIC STUDY:

Figure 3.4(a) shows the variation of the real part of the relative permittivity (ε') at different temperatures from 125 K to 300 K as a function of frequency in the range 100 Hz–1MHz. As we observed at a particular temperature, ε' decreases with increasing frequency and after attaining a certain high frequency it does not change. This behavior indicates that the dispersion is caused by Maxwell-Wagner (MW) interfacial polarization, which arises owing to the differing conduction mechanisms of grains and grain boundaries. [101,102] Moreover, in our systems, the temperature dependence of the ε' as a function of frequency are fingerprints of the MW effects. The low-frequency response of imaginary permittivity (ε'') is the key factor to differentiate the MW and Debye models (ε''): in a Debye system, $\varepsilon'' \rightarrow 0$ as frequency $\rightarrow 0$ while in the MW system, $\varepsilon'' \rightarrow \infty$ as frequency $\rightarrow 0$.[103] There are four fundamental polarization phenomena in materials that can be used to understand dielectric dispersion in general. They can be electronic, ionic, dipolar, and interfacial polarization and every polarization plays a significant role at particular frequencies. The

dielectric characteristic of BFO-based perovskite materials is dominated by interfacial and dipolar polarization at low frequencies, whereas ionic and electronic polarization dominates at higher frequencies[104]. It is obvious that in the low-frequency range (up to 10^3 Hz) the dielectric constant (ε') and dielectric loss (tan δ) reduce with increasing frequency as it is characteristic of dielectric materials, and thereafter became nearly constant at higher frequencies.[105] Dielectric relaxation is the source of the reduction in the dielectric constant. The Koop hypothesis[106] can be used to explain the dielectric dispersion. From this hypothesis the reduction in ε' with increasing frequency can be explained, the atoms in the dielectric material require a limited amount of time to align their orientations in the direction of the alternating applied electric field. When the frequency of the applied electric field attains a certain level, dielectric charge carriers are unable to follow it, and the value of the ε' drops. The value of dielectric constant values becomes constant at higher frequencies. We have performed the ε' measurements at different temperatures it has been observed that at room temperature the value of **ε'** is ~ 3400 which is quite high. The dielectric loss is shown in figure 3.4(b) for the present system follows the same pattern at a lower frequency and lower temperature range as the dielectric constant. The decrease in tanδ is explained by Koop's phenomenological model, which states that in the low-frequency region, when the grain boundary effect is dominant and the resistivity is high, the movement of electrons across Fe^{2+} and Fe^{3+} ions near grain boundaries consumes an excessive amount of energy, resulting in a high energy loss [107]. At high frequencies, when the resistivity is low and grains play a prominent role, just a tiny amount of energy is required for electron hopping between the Fe^{2+} and Fe^{3+} ions in the grain, and hence tanδ is negligible[108]. The BTFMO82 possesses a dielectric loss of around 1.25 at room temperature. This kind of behavior i.e. increment in a dielectric constant and low value of loss makes this material useful for high dielectric applications which we also reported

earlier for different systems[109].

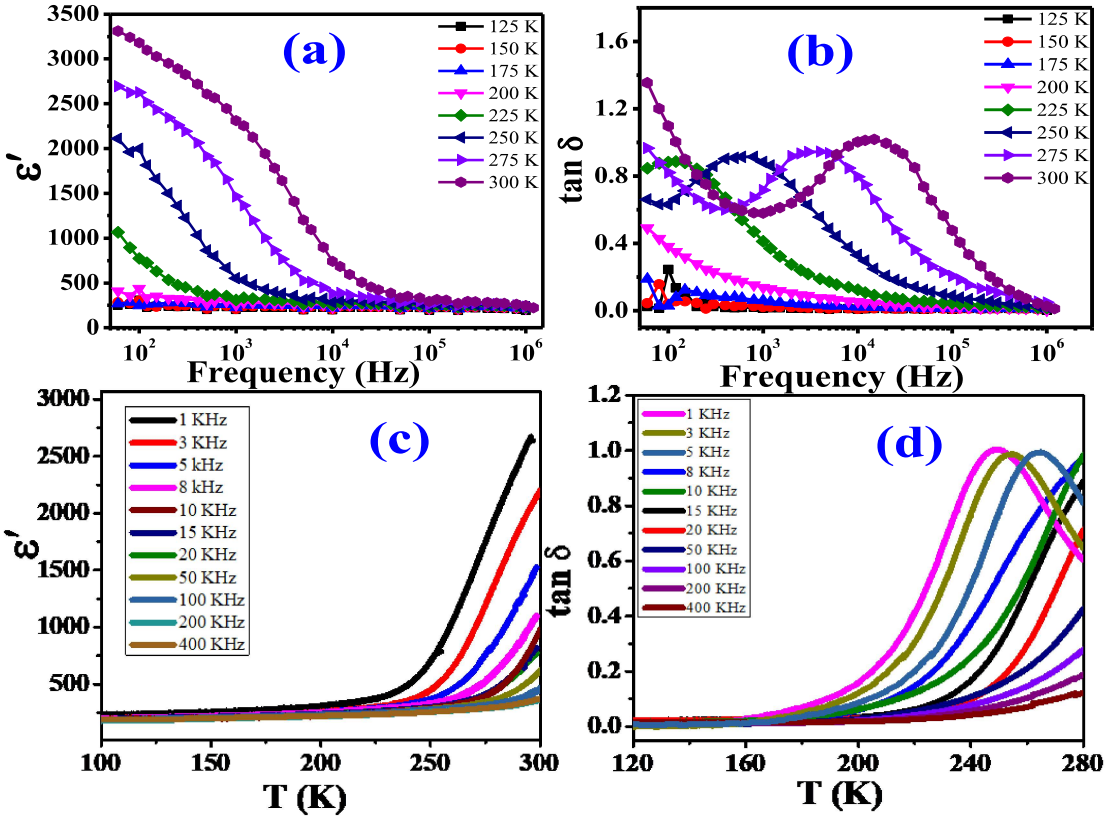

Figure 3.4: *Variation of (a) dielectric constant, and (b) dielectric loss with frequency at different temperatures. Variation of (c) dielectric constant, and (d) dielectric loss with the temperature at different frequencies.*

Furthermore, figure 3.4(c) shows the thermal variation of the dielectric constant of the real part and the dielectric loss factor at different frequencies in the temperature range 10 – 300 K. We observed no change in the dielectric constant till 225 K at all frequencies. As temperature increases above 225 K, there is a rise in the dielectric constant. The contribution of space charge (grain boundary and grain electrode surfaces) is reduced at high frequencies, enabling only the intrinsic dielectric constant of the grains to contribute to the measured value[110]. The real part of the dielectric permittivity has a step-like behavior and increases with increasing temperature. Thus, with increasing frequency, the steps shift

toward high temperature, in both the curves (loss and dielectric constant), indicating the typical relaxor behavior. The dielectric loss is less than one for our system at 1 kHz frequency as shown in figure 3.4(d). The low loss value of BFO-based material may be used for different application purposes.

For pure BFO dielectric constant value is low (55- 600) at room temperature and the dielectric loss value is very high [104,111–114] this restricts BFO from application purposes. We observed many folds of dielectric constant (i.e., 3400) values as compared to the reported BFO-based systems in the literature. A previous report by K. Saravana Kumar et al. shows that even the similar composition with different space groups reported also exhibited a smaller value of the dielectric constant (400 at room temperature)[115].

3.3.5 X-RAY PHOTOELECTRON SPECTROSCOPY STUDY:

It is important to have a previous understanding of the electronic structures of the current systems to comprehend their magnetic and dielectric characteristics. The oxygen vacancy may be the source of weak ferromagnetism, which contributes to the exchange bias in the current study. X-ray photoelectron spectroscopy (XPS) experiments were performed in the binding energy (BE) range of 0–1400 eV to determine the proportion of the element at the surfaces and the chemical constitution of the elements investigated in both systems using XPS. The XPS data were simulated and fitted using the XPSPEAK41 program to identify the valence states. The National Institute of Standard Technology (NIST) is assigned for all of the peaks, confirming the existence of Bi 4f, Tb 3d, Fe 2p, Mn 2p, and O 1s electronic levels in the system. It also indicates that the system is free of contaminants apart from carbon (C). C is found as it is absorbed by the sample surface during air exposure. The entire analysis was carried out after carbon correction, with the C1s line situated at BE 284.90eV for the BTFMO82 system to eliminate the charge effect error. Figure 3.5 (a-d)

shows the BE curve for constituting all elements present in the system. Bi core level splits into two main peaks $4f_{7/2}$ and $4f_{5/2}$ at BE 158.76eV, and 164.06eV for BTFMO82, demonstrating that Bi ions have the natural oxidation state of +3 as shown in figure 3.5(a). The energy difference between the Bi $4f_{7/2}$ and Bi $4f_{5/2}$ peaks was 5.3eV, which is consistent with previously reported experimental and theoretical results[116,117]. In Tb 3d, the most intense core level energy lies in the range of 1230eV and 1290eV energy for the sample shown in figure 3.5(b). Tb^{3+} ions $3d_{5/2}$ and $3d_{3/2}$BE are generally found at 1241eV and 1275eV, respectively, whereas Tb^{4+} binding energies are found at 1244 eV and 1278 eV. For our system, peaks associated with Tb^{3+} are at BE 1240.43eV and 1276.22eV, and related to Tb^{4+} are at BE 1243.34eV and 1278.59eV, respectively, and one satellite peak appears at 1249.03 eV. In our system, the existence of the mixed oxidation state of Tb^{3+} and Tb^{4+} is suggested by the peak position and doublet separation[118–120].

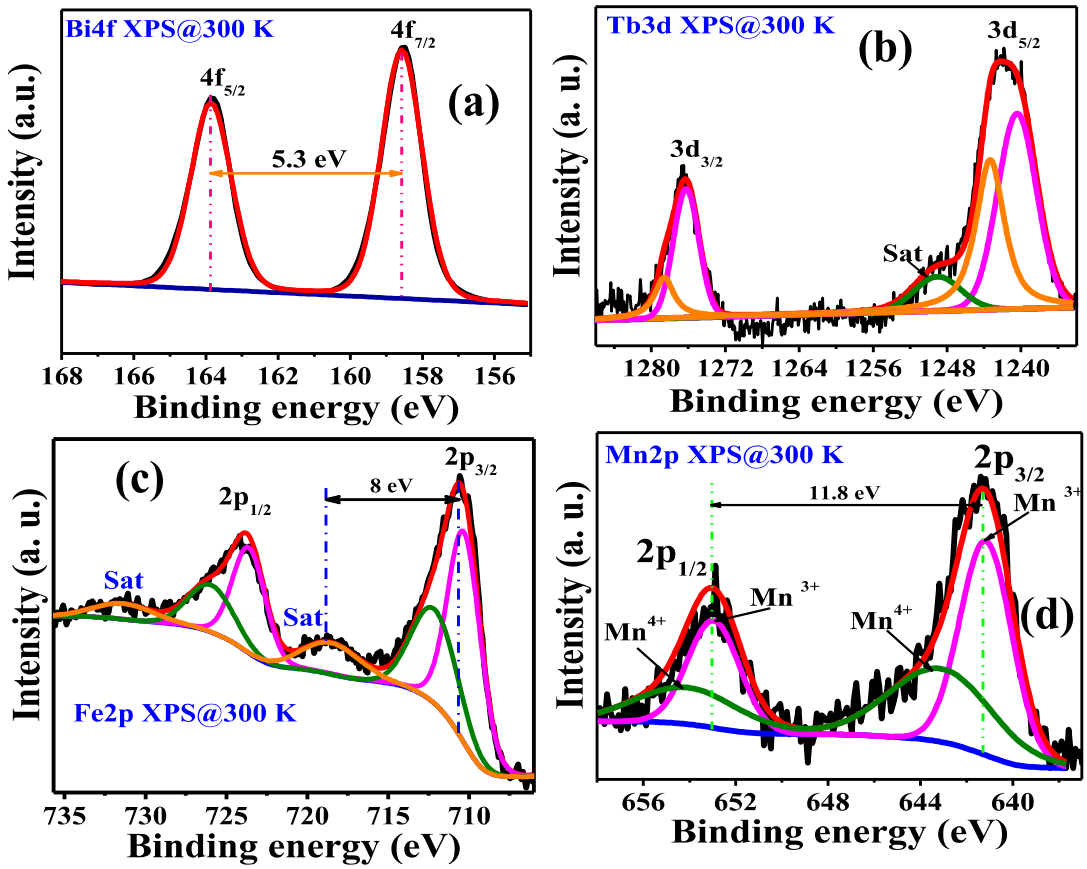

Figure 3.5: *X-ray photoelectron spectra of the (a) Bi 4f, (b) Tb 3d, (c) Fe 2p, and (d) Mn 2p for $Bi_{0.8}Tb_{0.2}Fe_{0.8}Mn_{0.2}O_3$ system at 300 K.*

The iron core level splits into two fundamental peaks for $2p_{3/2}$ and $2p_{1/2}$ because of the spin-orbit coupling shown in figure 3.5(c). The location of the Fe $2p_{3/2}$ peak is approximately 710eV, indicating that both Fe^{3+} and Fe^{2+} states coexist. The Fe $2p_{3/2}$ line of the system moves slightly to the higher BE implying a higher Fe^{3+} concentration. We observed 6 peaks deconvolution of Fe 2p at peak positions 710.3eV, 712.15eV, 718.33eV, 723.6eV, 725.95eV and 731.13eV. The major peak position of Fe $2p_{3/2}$ is at BE 710.5, which is in the range (710.06 – 711.2) eV and Fe $2p_{1/2}$ peak position is at 723.7eV[121]. The BE difference (spin-orbit splitting energy) between Fe $2p_{3/2}$ and Fe $2p_{1/2}$ peaks is 13.3eV for the system, which is in good agreement with the standard value of 13.6eV[122]. We observed two satellite peaks where the satellite peak of Fe $2p_{3/2}$ was positioned at 8 eV above the main peak confirming the Fe^{3+} valency in plenty[108,123]. Thus, the above discussion confirms that there is a larger ratio of Fe^{3+} than Fe^{2+} in the system. Nevertheless, the aforementioned results favor the mixed valency of Fe ions which is further supported by magnetic measurements. The two peaks are at 653.13eV ($Mn2p_{1/2}$) and 641.32eV ($Mn2p_{3/2}$), with a doublet spacing of ~ 11.8eV respectively for the sample. In Mn2p XPS spectra, MnO_2 has a doublet separation of 11.8eV, while Mn_2O_3 has a doublet separation of 11.6 eV (NIST).[124] We deconvoluted Mn2p XPS spectra for further confirmation of the oxidation states. Figure 3.5(d) shows the splitting of the Mn core level into two main peaks $Mn2p_{3/2}$ and $Mn2p_{1/2}$ because of spin-orbit coupling in the sample. The BE of Mn $2p_{3/2}$ is at 641.15 eV and 643.08 eV for the sample and $Mn2p_{1/2}$ is at 652.95 eV and 654.08 eV for the system. There is no satellite peak was observed thus indicating the mixed oxidation (Mn^{3+}, Mn^{4+}) state of Mn exists in our systems[94,124–128].

However, the Tb and Mn co-doping can effectively prevent the production of Fe^{2+} and the

volatilization of Bi^{3+} in BFO, resulting in a reduction in oxygen vacancy[129,130]. In the BFO structure, Fe^{3+} ions and low oxygen vacancies play an important role in magnetic properties. The Fe substitution of Mn not only suppresses spiral spin structure but also promotes a novel magnetic exchange mechanism between Fe^{3+}, Fe^{2+}, and Mn^{3+}, Mn^{4+} ions[88,131].

3.3.6 MAGNETIC STUDY:

Figure 3.6(a) illustrates the temperature variation of the dc magnetizations in zero-field cooled (ZFC) and field-cooled (FC) modes in a field of 100 Oe from 2 to 300 K. As the temperature drops, magnetization does not rise sharply while near 50 K, a sudden rise in the MT curve can be observed. In the present system, T_N shifted towards lower temperature as we doped Tb and Mn to the BFO at A and B sites respectively, as shown in the inset of fig 6(a). For pure BFO, T_N is around 643 K[132,133], which decreases to 521 K (inset of fig 3.5(a)) due to the co-doping of Mn and Tb. Figure 3.6(b) shows the M-H curve of the sample at 5 K and 300K temperatures in the absence of any applied external field (H) (H=0, ZFC). At room temperature, the M-H loop exhibits an almost linear change in magnetization with an external applied magnetic field, which is characteristic of an AFM material. A nonlinearity deviation is seen in the vicinity of the zero fields, which suggests the presence of FM ordering as well, which is shown in the inset of fig. 5(b) at 300 and 5 K temperatures. The moment value at room temperature for BTFMO82 is 1.81 emu/g which is larger than the pure BFO ($\leq$0.5 emu/g) system[82,134].

However, further study is needed to understand this type of behavior for the M-H loop. Additionally, a detailed study of the area surrounding the zero field (inset fig. 3.5(b)) indicates that the loops, measured at 300 K and 5 K are asymmetrical in character suggesting the existence of exchange bias (EB) for the BTFMO82 system. This kind of

shift in the hysteresis loop at zero applied fields is known as spontaneous exchange bias (H_{SEB}). A ferromagnetic (FM) unidirectional anisotropy produced at the interface between different magnetic phases is considered to produce the EB effect. Coercivity is denoted as $H_C = |H_L - H_R|/2$, and the exchange bias field is defined as $H_{EB} = |H_L + H_R|/2$, where H_L and H_R are left and right coercive

fields, respectively, are used to represent the shift. Under the ZFC situation, spontaneous exchange bias (H_{SEB}) was approximately 468 Oe and 11.04 Oe, and H_C from the ZFC loop is around 349 Oe and 38.04 Oe at 300 K and 5K temperatures respectively. Generally, EB increases as temperature reduces[76] whereas, we observed the EB increases as temperature increases i.e., our material exchange bias value is high at room temperature as compared to 5K temperature which follows the similar behavior as our earlier report[135]. The following studies have been carried out to better understand the observed exchange bias and its temperature variation.

Figure 3.6(c) shows the comparative hysteresis loop study of our system with ZFC (H_{SEB}) and FC (at H_{FC} = 5T; H_{CEB}) at room temperature. In the inset of figure 3.6(c), we can see that there is more hysteresis shift at the 0T field (H_{SEB}), as compared to the 5T applied field, at the 5T EB value reduced. This type of spontaneous exchange bias was also found in $BiFeO_3$ (AFM) - $CoFe_2O_4$ (Ferrimagnetic; FiM) nanocomposite prepared by Huang et al. and they explained that with increasing applied field the FiM clusters grow and as a result, the proportional percentage between the Ferrimagnetic to the AFM clusters gets reduced.[72] The enormous moments of the FiM area can't be pinned by the AFM modest spins. This phenomenon is analogous to the FM/AFM bilayer system, in which the EB vanishes when the AFM layer thickness falls below a critical value, and the H_{EB} is roughly inversely proportional to the FM layer thickness ($H_{EB} \propto 1/t_{FM}$), as a result, the EB effect became less

effective (i.e. H_{EB} decreases) as the thickness of FM layer increases [136].

Perovskite cobaltite $La_{1-x}Sr_xCoO_3$ exhibits a similar behavior where the EB effect decreases with increased measure field and the exchange bias phenomenon disappeared as a high field is applied which supports our study [137]. Figure 3.6(d) illustrates the M-H graph obtained using two distinct measurement techniques P-type (-5 T) and N-type (+5T) applied field. The observed spontaneous M–H loop alterations are not an artifact of the experiment, but rather a system characteristic[138]. P-type measurements have a negative shift along the field axis, while N-type measurements have a positive shift[78]. To understand the exchange bias behavior in our system, we perform thermoremanent magnetization (TRM) measurements as explained in the literature.[75,76,127] TRM (moment *vs*. the field (H)) measurement has recently been used as a fingerprinting technique to distinguish different magnetic states such as spin glass, DAFF, and others as they can identify the nature of irreversible magnetization contributions.

Figure 3.6(d) inset (upper) shows the TRM study which increases monotonically as observed for DAFF-type systems.[75] TRM is measured by applying a field and cooling till the required temperature and then the field is released, and the magnetization was instantly recorded. To understand the possible mechanism of the EB phenomenon in the BFO-based system many research groups demonstrated many different types of the mechanism under FC. Benitez et al[75] got the same behavior as we observed for our system. Manna et al.[76] and Dong et al. [139], also explained the existence of a surface shell with DAFF and AFM core for $BiFe_{0.8}Mn_{0.2}O_3$ nanoparticles, they also referenced the dilution of the AFM layer because of non-magnetic material doping and they got similar TRM behavior.

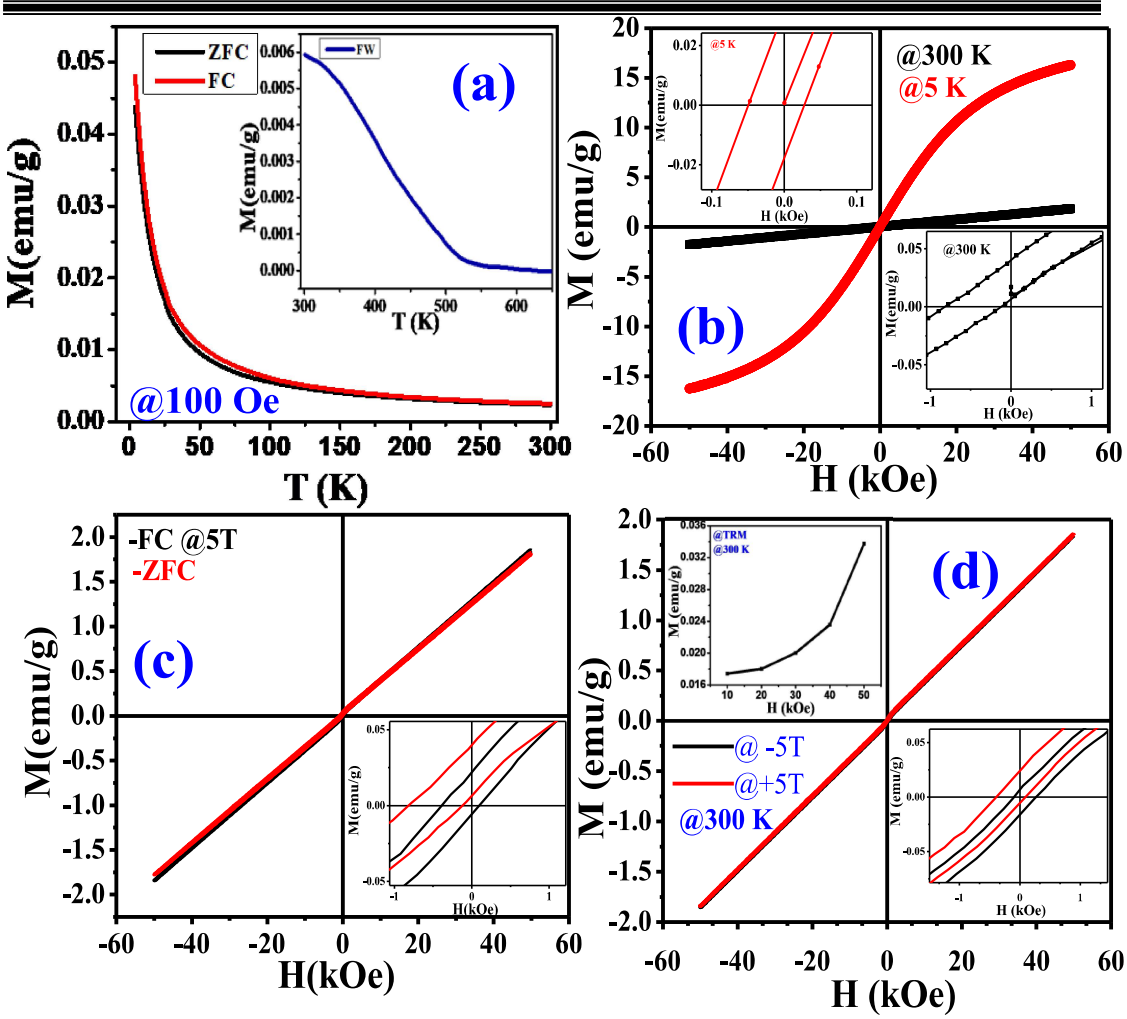

Figure 3.6: *(a) Moment vs. temperature curves measured for zero field cooling and field cooling conditions at 100 Oe in the temperature range 5 K – 300K. The inset demonstrates field warming data from 300K – 840 K temperature. (b) The hysteresis loop shift, signifying the spontaneous exchange bias at 5 K and 300 K is measured under zero-field cooling conditions. In the inset, we have shown the extended view of the spontaneous exchange bias. (c) Comparison between conventional exchange bias (field cooling at 5 T) and spontaneous exchange bias at room temperature. In the inset, we have shown the extended view. (d) Conventional exchange bias was measured at -5T and +5T. Thermoremanent magnetization vs. field variation is shown in the inset.*

Zhang et al. showed pictorially and gave the region for core AFM and DAFF shell-type mechanism in their nanocrystal of BFO. They mentioned that because of lattice distortion the Fe-O-Fe bond angles are changed (from neutron study) which may destroy the AFM interaction and the coexistence of mixed valency (from XPS study) of Fe can also explain this phenomenon.[140]

Moreover, the XPS study suggests the existence of mixed-valence states of both Fe (as Fe^{3+} and Fe^{2+}) and Mn (Mn^{3+}, Mn^{4+}), as a result, there are many different types of interactions.[88,108]This might be the reason for observed spontaneous exchange bias in BFO-based systems which are rare and useful in memory devices and many other applications. S. Yakout at el. explained the importance of devices based on spintronics proposed to execute all functions, including data processing and storage.[1] From the studied literature and our EB data, we can explain with the help of a phenomenological qualitative model with the framework of the 2D DAFF shell and AFM core structure as discussed by Zhang et al. that at RT with increasing field at interface volume, the FM type spins in DAFF shell increases as compared to AFM type spins and as a result, H_{CEB} decreases as applied field increases.[127] To the best of our knowledge, room temperature spontaneous exchange bias in the BFO base system is absent in the literature, thus making BTFMO82 can be an essential element to make memory devices. Moreover, the magnetic moment of our system also increases at room temperature and even at low temperatures (i.e., 5K) as compared with other systems.[141,142] The TRM measurement behavior is similar to those already reported in nano-size materials (discussed in earlier references) and previously we have also reported the exchange bias phenomenon in bulk $0.7BiFeO_3$-$0.3TbMnO_3$ composite which support this study[143]. Different research groups discussed different types of compositions (i.e., about EB) from all this literature survey and the $Bi_{0.8}Tb_{0.2}Fe_{0.8}Mn_{0.2}O_3$ TRM study confirms that in this system 2-dimensional DAFF layer is present. It is worthwhile to mention here, that the observation of room temperature spontaneous exchange bias in a BFO-based system is still rare and thus placing our system in the rare materials.

3.4 CONCLUSION

In conclusion, the structural, dielectric, and magnetic properties of the polycrystalline

$Bi_{0.8}Tb_{0.2}Fe_{0.8}Mn_{0.2}O_3$ system have been studied elaborately. A structural shift from the rhombohedral (space group R3c) to the orthorhombic (space group Pn21a+Pnma) phase has been confirmed by structural analysis. Interestingly, the neutron powder diffraction study supports the XRD study. There is a non-zero magnetic moment at room temperature which confirms that the $Bi_{0.8}Tb_{0.2}Fe_{0.8}Mn_{0.2}O_3$ has ferromagnetic type ordering at room temperature. More interestingly, with the substitution of Mn and Tb in BFO, the value of the dielectric constant increases and the dielectric loss value decreases. The larger value of the dielectric constant suggests that these types of materials can be used for high-dielectric applications. However, we observed that the emergence of Maxwell-Wagner behavior was related to the increase in the dielectric constant. The presence of Bi, Tb, Fe, and Mn elements in the sample is shown by XPS analysis, we found the mixed-valence state of Tb (+3, +4), Fe (+2, +3), and Mn (+3, +4) elements. There are different types of exchange interaction between all these mixed valence elements which can induce the exchange bias phenomenon in our system. The value of spontaneous exchange bias is higher than that of conventional exchange bias at room temperature, which is rare in a BFO-based system. The Neel temperature reduces to 521 K from 643 K for this system, and the magnetization value also increases. This system is composed of an AFM core and a 2-dimensional DAFF layer with a net magnetization under the field, according to neutron diffraction and TRM data. Furthermore, the $Bi_{0.8}Tb_{0.2}Fe_{0.8}Mn_{0.2}O_3$ system shows reasonable H_{EB} and H_C values at room temperature making it intriguing and appealing for a variety of multifunctional devices. The intriguing discoveries of this spontaneous exchange bias effect in such perovskite system at room temperature might lead to new technical innovations in the future.